Plasmonic Core–Satellite Assemblies as Highly Sensitive Refractive Index Sensors

ARTICLE *in* THE JOURNAL OF PHYSICAL CHEMISTRY C · MARCH 2015

Impact Factor: 4.77 · DOI: 10.1021/jp510985n

THE JOURNAL OF PHYSICAL CHEMISTRY C

Article

pubs.acs.org/JPCC

Plasmonic Core–Satellite Assemblies as Highly Sensitive Refractive Index Sensors

Janak Prasad,[†,‡] Inga Zins,[†,‡] Robert Branscheid,[†] Jan Becker,[†] Amelie H. R. Koch,[§] George Fytas,[§,∥] Ute Kolb,[†] and Carsten Sönnichsen*[,†]

[†]Institute of Physical Chemistry, University of Mainz, Duesbergweg 10-14, D-55128 Mainz, Germany

[‡]Graduate School Materials Science in Mainz, University of Mainz, Staudingerweg 9, D-55128 Mainz, Germany

[§]Max Planck Institute for Polymer Research, University of Mainz, Ackermannweg 10, 55128 Mainz, Germany

[∥]Department of Materials Science, University of Crete and IESL/FORTH, 71110 Heraklion, Greece

Supporting Information

ABSTRACT: Highly sensitive and spectrally tunable plasmonic nanostructures are of great demand for applications such as SERS and parallel biosensing. However, there is a lack of such nanostructures for the midvisible spectral regions as most available chemically stable nanostructures offer high sensitivity in the red to far red spectrum. In this work, we report the assembly of highly sensitive nanoparticle structures using a hydroxylamine mediated core–satellite assembly of 20 nm gold nanoparticle satellites onto 60 nm spherical gold cores. The average number of satellites allows tuning the plasmon resonance wavelength from 543 to 575 nm. The core–satellite nanostructures are stable in pH ranges from 5 to 9 and show about 2-fold higher plasmonic sensitivity than similar sized gold nanospheres.

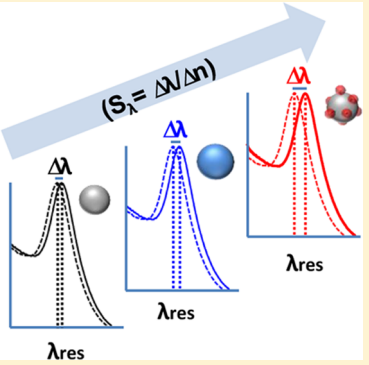

INTRODUCTION

Gold nanoparticles have been exploited as novel nanoscopic sensor elements in recent years, both in surface enhanced Raman scattering (SERS)[1] and plasmon shift based refractometric sensors.[2,3] For the latter, refractive index changes Δn in the nanoparticle environment are detected via the induced plasmon resonance shift $\Delta\lambda$.[4] Finding highly sensitive metal nanostructures (with large values of $S_\lambda = \Delta\lambda/\Delta n$) has been an area of importance in this field. High sensitivity can be achieved by tailoring the size and shape of particles, using for example nanospheres, nanocubes, bipyramids, and nanorods[5,6] or more complex geometries such as nanobranches,[7] nanorattles,[8] nanoshells,[9] nanoflowers,[10] and nanotubes.[11] However, the plasmon resonances of most of the above structures are in the red to NIR region of the electromagnetic spectrum. For some applications (e.g., multiplexing),[12] it is desirable to have plasmonic structures with high sensitivity in the midvisible (green to red) part of the spectrum. Here we show a novel strategy for batch synthesis of core–satellites structures that offer high sensitivity in the midvisible. The core–satellite structures are nearly 2-fold more sensitive than gold nanospheres alone. Its refractive index sensitivity is also notably higher than gold nanocubes (λ_{max} = 538 nm).[5] Moreover, the resonance wavelength of core–satellites can be tuned from 543 to 575 nm by adjusting the number of satellites. These nanostructures will be useful for various plasmonic applications like SERS,[13] multiplexed analyte detection,[14] and colorimetric sensing.[15]

Controlled assembly of gold nanoparticles into dimers,[16] trimers,[17] and core–satellites[18,19] is an effective means to increase[20] their Raman scattering enhancement by a factor of 10^8–10^{11}. The accepted reason is that these nanostructures have sharper apexes and a gap which allow a large part of the plasmon field to penetrate the dielectric environment.[8] The same mechanism should improve the plasmonic sensitivity S_λ of core–satellites. The number of hot spots and the resonance position of core–satellites can be tuned by varying the satellite number, core and satellite size, and the interparticle distance.[21,22] Sensitivity of core–satellites is inversely related to the coupling distance between the core and the satellites.[21] Conventionally, DNA has been used as a molecule of choice for creating core–satellite nanostructures.[13,23,24] Since DNA sequences used in these cases require a certain minimal length to ensure proper base pairing, the intra-assembly gap distances reach tens of nanometers. Moreover, the distances between core and satellites are difficult to specify due to nonspecific adsorption of nitrogenous bases of DNA onto gold nanoparticles.[25] Other small molecules[15,18,20] have been shown to assemble core–satellites onto a substrate, but in solution phase batch synthesis, these molecules produce a low yield of core–satellites. Recently, *p*-aminothiophenol has been used to electrostatically drive the formation of core–satellites in

Received: November 2, 2014
Revised: February 6, 2015
Published: February 11, 2015

DOI: 10.1021/jp510985n
J. Phys. Chem. C 2015, 119, 5577–5582

solution.[26] These assemblies have much shorter gap distances, but they have a tendency to destabilize at near neutral or higher pH.

In our approach, we deposit 20 nm citrate capped gold nanosphere satellites on methoxy-PEG functionalized 60 nm gold nanosphere cores (Figure 1). The process contains a long

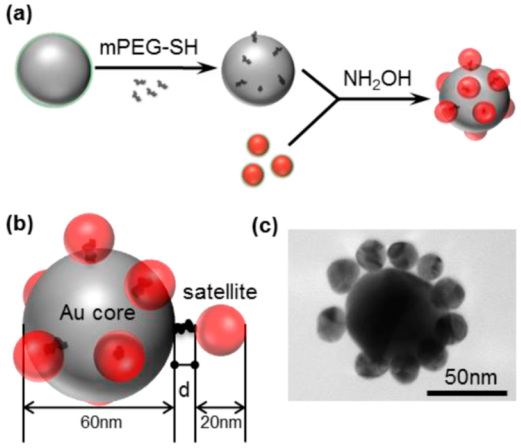

Figure 1. (a) Schematics of the core−satellite formation procedure. (b) The citrate stabilized 20 nm satellite nanospheres are attached to PEGylated 60 nm gold core with a gap distance *d*. (c) Representative TEM image of the assembled structure.

coincubation period followed by the addition of hydroxylamine (see methods section). Shortly after the hydroxylamine addition, the core−satellite assemblies have formed in high yield (>98%, see TEM image in Figure 1c). The mechanism of assembly involves charge neutralization of citrate coated spheres with hydroxylamine, causing these particles to partially lose their colloidal stability and subsequently adsorb onto the methoxy-PEG functionalized core particles (see the Supporting Information, Figure S1). This simple approach for the batch synthesis of core−satellite nanostructures in high yield avoids many of the above-mentioned complications.

EXPERIMENTAL METHODS

Synthesis of Core−Satellite Nanostructures. Gold core−satellite structures (Au-CS) were assembled by a novel "hydroxylamine mediated assembly method". In a typical procedure, we centrifuged 500 μL of large citrate stabilized gold spheres (60 nm, BBI International) at 2460g for 5 min and resuspended them in 200 μL of 2 mM mPEG-SH (5000g/mol, Iris Biotech). The mixture was incubated overnight at room temperature to ensure complete PEGylation. To remove excess unbound PEG molecules, the particles were centrifuged down at 4820g for 5 min, leaving a pellet of PEGylated gold nanoparticles at the bottom. The pellet was resuspended twice in 200 μL of deionized water and centrifuged down (at 4820g for 5 min). After the last washing step, the pellet was diluted with 30 μL of water. Three such batches were prepared. Deionized water from a Millipore system (Milli-Q) was used throughout. Next, 270 μL of small citrate stabilized gold spheres (20 nm, BBI International) were centrifuged in a separate microfuge tube at 4820g for 10 min and the pellet was diluted in 10 μL of deionized water. Again three such batches were prepared. Each batch of 10 μL 20 nm gold spheres was mixed together with a partner batch of 30 μL PEGylated 60 nm cores and vigorously stirred and incubated overnight on a shaking table. Finally, nanoparticle assembly into core−satellites was induced by adding 0.5, 0.75, and 1.0 μL of 70 mM hydroxylamine into these three batches. All three samples were diluted to 100 μL after 10 min of reaction. After 1 h, the volume of the reaction mixture was further diluted to 500 μL with water to deactivate the remaining traces of hydroxylamine.

Particle Characterization. Optical extinction spectra ("UV−vis") of core−satellite nanostructures (Au-CS), mPEG5000g/mol functionalized 60 nm gold spheres (60 nm cores), and mPEG500g/mol functionalized 80 nm gold spheres (80 nm cores) were recorded with a fiber optic spectrometer (Ocean Optics, USB2000) coupled to a tungsten light source (Ocean Optics, FL-2000-FHSA) using a Spectro Pipetter (Ocean Optics). Low-resolution TEM images and Cryo-TEM images of the core−satellite samples were acquired to investigate the number of satellites on core particles. Transmission electron microscopy measurements were performed on a Tecnai F30 ST at 300 kV in imaging mode. Cryo-TEM images were taken using a Fischione Cryo-transfer tomography sample holder from aqueous samples vitrified with a FEI Vitrobot. Electrophoretic mobility of the core−satellite structures was determined in 0.3% Agarose gels (chamber length 0.145 m, 1034.5 V/m, 30 min) to verify the assembly strength under dynamic conditions. The pH measurements were performed with Sartorius Professional Meter PP 20. Photon correlation spectroscopy, both polarized and depolarized (PCS),[27] was used to record the hydrodynamic radius (R_h) and rotational radius (R_r) of 60 nm cores in different water−glycerol mixtures.

Ensemble Sensitivity Measurements. A quantitative comparison of the refractive index sensitivity of Au-CS, 60 nm cores and 80 nm cores was performed by systematically varying the refractive index of the solvent. To vary the refractive index, different water−glycerol mixtures were prepared. The refractive index (n) of the solvent was checked with a digital refractometer (Refracto 30PX).The plasmon resonance wavelength (λ_{res}) of the nanoparticles was determined for several changes in refractive index (n) with the fiber-optic spectrometer. The slope of the resulting linear trend gives the ensemble sensitivity of the nanostructures ($S_\lambda = \Delta\lambda_{res}/\Delta n$).

Single Particle Spectroscopy. To record the plasmon shifts ($\Delta\lambda_{res}$) of single nanoparticles, we use a dark-field microscope coupled to a spatially addressable liquid crystal display as an entrance to an imaging spectrometer, which allows the simultaneous investigation of many particles with high temporal resolutions (fastSPS).[28] The typical procedure involved rinsing a 1:20 diluted suspension of the nanoparticles for 5 min through a flat glass capillary connected to PET tubing. Subsequent rinsing with 1 M NaCl solution for another 40 min immobilized the particles on the capillary walls. The glass capillary was then rinsed for 20 min with Milli-Q water to remove excess salt and loosely bound particles. Now the setup recorded the reference scattering spectra of all the particles in the field of view, followed by a cyclic rinsing of the flow cell with water−glycerol mixtures having refractive indices of 1.34 and 1.38. In every cycle, the corresponding spectral shifts of each individual particle in the field of view were recorded. Only fully reversible spectral shifts were considered to quantify plasmonic sensitivity.

RESULTS AND DISCUSSION

The satellites should bind at random sites on the PEG layer around the core-particles. However, traditional TEM images (as

DOI: 10.1021/jp510985n
J. Phys. Chem. C 2015, 119, 5577−5582

in Figure 1b) of dried samples typically showed a "flower-like" pattern due to the collapse of the PEG shell upon drying. To observe the arrangement as it is present in solution, we used Cryo-TEM, where a thin layer of the solution is so rapidly frozen that the native structure is preserved. Figure 2 shows

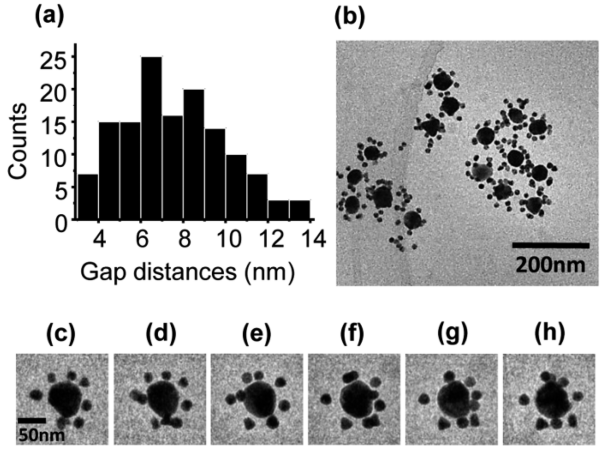

Figure 2. (a) Histogram of (projected) gap distances d between satellites and cores measured on Cryo-TEM images (b) at a fixed tilt angle. A single nanostructure is imaged at different tilt angles (c–h) demonstrating that even satellites appearing almost touching in one projection actually sit at a distance from the core.

TEM images obtained on such a frozen sample under various tilt angles (additional image sequences are available as movies in the Supporting Information). The cryo-images in Figure 2 and the movies conclusively demonstrate that the actual structure in solution is indeed a random arrangement of satellites around a core particle. Furthermore, we observed a clear spacing (of ~7 nm) between satellites and cores (contrary to the collapsed "flower" structures). Because the Cryo-TEM images show a projection of the randomly oriented satellites, the end-to-end gap distances shown in Figure 2a are only a lower limit to the actual distances. However, by tilting an individual assembly over a wide range of angles, we could demonstrate that even satellites appearing to touch the core in one projection are actually spaced some distance apart (see Figure 2c–h).

The average number of satellites per core particle can be precisely tuned by varying the concentration of hydroxylamine. Technically, it is much easier to adjust the concentration of hydroxylamine than the concentrations of nanoparticles (core or satellites) because their concentration can only be estimated indirectly. Final hydroxylamine concentrations of 70, 105, and 140 μM lead to an average of 3, 7, and 8 satellites per core (Figure 3a) as determined by TEM (Figure 3b–d). Here, on the dried sample, we counted a satellite as belonging to a core particle only if the satellite is present at a distance of <5 nm from the core in the TEM image. In a Cryo-TEM micrograph, where the PEG spacing is apparent between the core and its satellites, this distance can be approximated to the hydrodynamic diameter of the PEG layer (~18 nm, as measured by PCS). The yield of core–satellites was >98% (Figure 3a and in the Supporting Information, Figure S2). The last value (8) is only a lower limit because not all satellites could be counted due to core–satellite–core fusion. For the highest hydroxylamine concentration (Figure 3d), we observed a considerable amount of uncontrolled clustering that made us cautious to use even higher hydroxylamine concentrations. The corresponding optical resonance maxima (λ_{max}) are at 543, 551, and 575 nm, respectively (Figure 3e). The observed trend (higher spectral shift on increasing numbers of satellites) is expected because of increased plasmon coupling. Apart from the plasmon resonance maxima, the electrophoretic mobility of the core–satellites also depends on the number of satellites (Figure 3f). For the higher number of satellites, the mobility decreases as expected from the combined effect of surface charge neutralization and increasing size.[29] We hypothesize that only a partial reduction in surface charge on citrate stabilized satellites takes place in the

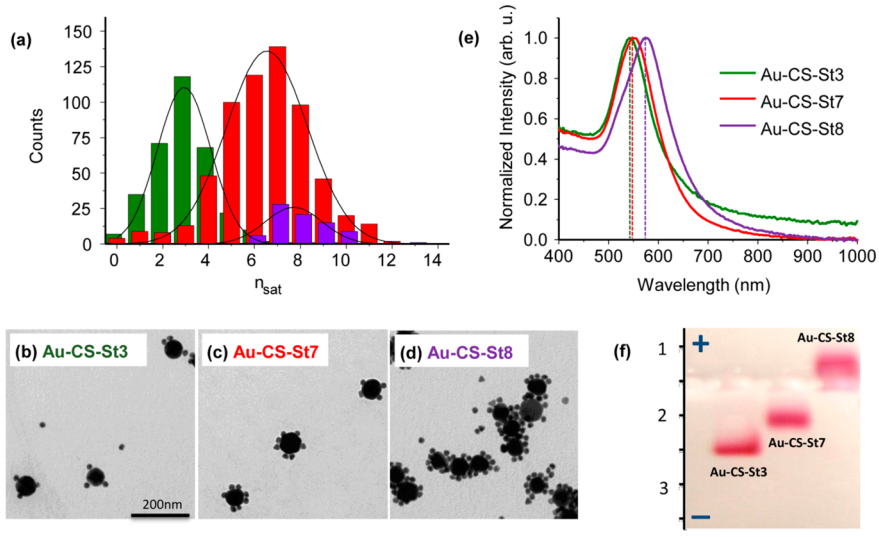

Figure 3. (a) Histogramm of the number of satellites per core. A Gaussian fit of the distribution leads to a median number of 3, 7, and 8 (in the last case, all satellites could not be counted due to significant levels of core–satellite–core fusion) satellites per core for Au–CS–St3 (green), Au–CS–St7 (red), and Au–CS–St8 (violet), respectively. (b–d) Electron-microscopy images of typical core–satellite samples (all images have the same magnification). (e) Ensemble-spectra of the different core–satellite assemblies with increasing satellite number showing the red-shift with increasing number of satellites. (f) Agarose gel-electrophoresis (0.3% agarose, 0.5× TBE, 150 V, 30 min) of 60 nm mPEG-coated spheres and three core–satellite preparations showing the lower mobility of assemblies with larger number of satellites.

DOI: 10.1021/jp510985n
J. Phys. Chem. C 2015, 119, 5577–5582

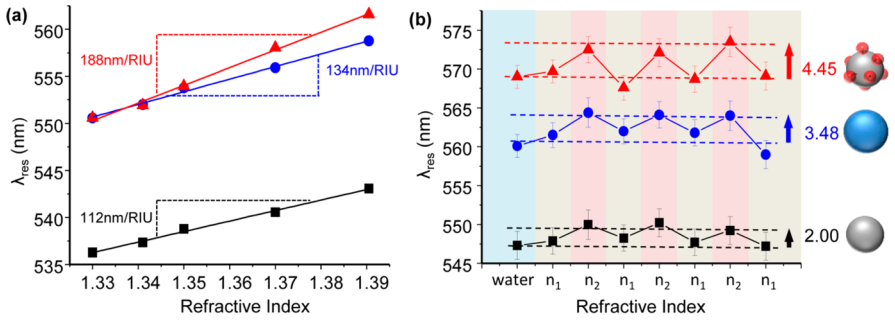

Figure 4. (a) Ensemble resonance position of 60 nm cores (black), 80 nm cores (blue), and core satellite assemblies (Au−CS−St7, red) in different refractive index media. The slope of the linear fit corresponds to the ensemble sensitivity of 112, 134, and 188 nm/RIU, respectively. (b) Median resonance position from single-particle measurements of 60 nm cores (black), 80 nm cores (blue), and Au−CS−St7 (red) in refractive index media 1.34 (n_1) and 1.38 (n_2). The shift of the resonance wavelength shows good reversibility. The median shifts are 2.00, 3.48, and 4.45 nm. The error bars represent the standard deviation of the spectral shift observed in the resonance position of 30 different particles.

Table 1. Plasmon Sensitivities S_λ and Figure of Merit (FOM) for the Core−Satellite Nanostructures Compared to PEGylated Cores

nanostructure type	S_λ (ensemble)	S_λ (single particles)	FOM (single particles)
60 nm cores	112	50 ± 8.5	0.69
80 nm cores	134	87 ± 13.7	0.99
60 nm core − 20 nm satellite	188	111 ± 49	1.80

presence of hydroxylamine (see the Supporting Information, Table S2). Thus, the spheres still remain slightly negatively charged and this charge tends to build up as the satellite count per core increases. At a higher number of satellites per core, the nanostructures perhaps overcome the charge on to the PEG layer and tend to migrate toward the negative pole during gel electrophoresis. Core−satellites demonstrate excellent stability and robustness under electrophoretic conditions. Furthermore, they are also fairly stable at high ionic strengths of up to 1 M NaCl and within the pH range of 4−9 (see the Supporting Information, Figure S3 and S4).

Our motivation to make core−satellite gold nanoparticle structures was their potential use as plasmon sensors. One of the most important parameters characterizing plasmon nanosensors is their sensitivity to refractive index changes in the surroundings. The sensitivity S_λ is defined as the shift in the plasmon resonance wavelength $\Delta\lambda_{res}$ per unit change in the surrounding refractive index Δn ($S_\lambda = \Delta\lambda_{res}/\Delta n$). We measured the sensitivity S_λ for 60 nm cores, 80 nm cores, and core satellite structures (with 60 nm cores and an average of 7 satellites with 20 nm diameter) by systematically changing the solvent refractive index using a water−glycerol mixture (Figure 4a). The sensitivity of 60 nm cores was much lower (112 nm/RIU) than the sensitivity for core−satellite structures with the same core (188 nm/RIU). It is well-known that plasmon sensitivity increases with resonance wavelength.[30] Due to this fact, we also included 80 nm cores that show approximately the same resonance wavelength (see the Supporting Information, Figure S5). However, their plasmon sensitivity S_λ was only 134 nm/RIU, still lower than the core−satellite structure. The core−satellites also demonstrate a 2-fold higher sensitivity than gold nanocubes (S_λ = 83).[5]

To make sure that a solvent-mediated collapse of the intermediate PEG layer is not the reason for the observed plasmon shift of core−satellite structures when adding glycerol, we measured both the hydrodynamic radius (R_h) and rotational radius (R_r) of 60 nm cores in different water−glycerol mixtures with polarized and depolarized photon correlation spectroscopy, respectively;[27] the latter is more sensitive to possible conformational change of the PEG layer due to the R_r^3 dependence of the rotational diffusion. When correcting for the measured viscosity of the solvent, no significant glycerol dependent change in the hydrodynamic radius was observed (see the Supporting Information, Figure S6 and Table S1).

One of the most promising applications of plasmon sensors is their use in single nanoparticle experiments. In such experiments, the extremely small sensing volume is taken advantage of in an optimal way. To investigate if the above results hold true for single particle measurements, we investigated the plasmon sensitivity for the same three samples as above on single particles immobilized inside of a glass capillary. The immobilization allows a repeated change of the surrounding solution (from n = 1.34 to 1.38 and back)—something we found generally to be very important when determining plasmon sensitivity as reversible effects due to changes in the environment can be discriminated from irreversible shifts caused by changes to the particles themselves.[31] In this case, however, the shifts were fully reversible, which allows us to extract meaningful plasmon sensitivity values (Figure 4b and the Supporting Information, Figure S7). The average values obtained on about 30 nanoparticles per sample are slightly smaller than that for ensemble measurements as expected from the partial blocking of the particle surrounding by the substrate. The extracted values are $\Delta\lambda_{res}$ = 2.00 ± 0.34 nm, $\Delta\lambda_{res}$ = 3.48 ± 0.55 nm, and $\Delta\lambda_{res}$ = 4.45 ± 1.97 nm yielding sensitivities and figure of merit (FOM = S_λ/plasmon line width) as summarized in Table 1. The increase in the FOM for core−satellites reflects the increase in plasmon sensitivity and almost unchanged plasmon line width (fwhm) of the 60 nm cores after assembly with the satellites.

■ CONCLUSION

In both cases, ensemble and single particle measurements, the plasmonic sensitivity of core−satellite structures proved to be larger than that of similar sized spherical particles (with

DOI: 10.1021/jp510985n
J. Phys. Chem. C 2015, 119, 5577−5582

comparable spectral position). We believe that the enhanced sensitivity results from a larger part of the electromagnetic field connecting the induced surface charges penetrating the surrounding environment accessible to the solvent molecules—similar to the case of hollow nanorattles reported before.[8] The advantage of core−satellite structures to other high sensitivity plasmon sensors is their relatively straightforward assembly that allows a simple fine-tuning of the desired resonance wavelength by adjusting the average number of satellites. Another potential advantage is the possibility to include responsive polymers as linkers which would drastically enhance the spectrum of measurable parameters (for example, temperature, pH, specific ligands, and ions). Potentially, our assembly route could be extended to nanoparticles with different materials, for example, using magnetic nanoparticles,[32] for multiplexed labeling, drug delivery, SERS enhancement, or completely novel physical effects.

■ ASSOCIATED CONTENT

Supporting Information

Additional experimental results to elucidate the mechanism of core−satellite assembly (Figure S1 and Table S2), to determine the stability of core−satellites (Figures S3 and S4), for the spectral analysis of the resulting nanostructures (Figures S5 and S7), and to verify the absence of interaction between PEG linker and the surrounding medium (Table S1); additional TEM image sequences as movies. This material is available free of charge via the Internet at http://pubs.acs.org.

■ AUTHOR INFORMATION

Corresponding Author

*E-mail: soennichsen@uni-mainz.de.

Author Contributions

The manuscript was written through contributions of all authors. All authors have given approval on the final version of the manuscript.

Notes

The authors declare no competing financial interest.

■ ACKNOWLEDGMENTS

This work was financially supported by the ERC grant 259640 ("SingleSense"). J.P. and I.Z. were financially supported by the graduate school of excellence Materials Science in Mainz.

■ REFERENCES

(1) Haes, A. J.; Haynes, C. L.; McFarland, A. D.; Schatz, G. C.; Van Duyne, R. P.; Zou, S. Plasmonic Materials for Surface-Enhanced Sensing and Spectroscopy. *MRS Bull.* **2005**, *30*, 368−375.

(2) Anker, J. N.; Hall, W. P.; Lyandres, O.; Shah, N. C.; Zhao, J.; Van Duyne, R. P. Biosensing with Plasmonic Nanosensors. *Nat. Mater.* **2008**, *7*, 442−453.

(3) Jain, P.; Huang, X.; El-Sayed, I.; El-Sayed, M. Review of Some Interesting Surface Plasmon Resonance-Enhanced Properties of Noble Metal Nanoparticles and Their Applications to Biosystems. *Plasmonics* **2007**, *2*, 107−118.

(4) Mock, J. J.; Smith, D. R.; Schultz, S. Local Refractive Index Dependence of Plasmon Resonance Spectra from Individual Nanoparticles. *Nano Lett.* **2003**, *3*, 485−491.

(5) Chen, H.; Kou, X.; Yang, Z.; Ni, W.; Wang, J. Shape- and Size-Dependent Refractive Index Sensitivity of Gold Nanoparticles. *Langmuir* **2008**, *24*, 5233−5237.

(6) Lee, K. S.; El-Sayed, M. A. Gold and Silver Nanoparticles in Sensing and Imaging: Sensitivity of Plasmon Response to Size, Shape, and Metal Composition. *J. Phys. Chem. B* **2006**, *110*, 19220−19225.

(7) Chen, H.; Shao, L.; Woo, K. C.; Ming, T.; Lin, H. Q.; Wang, J. Shape-Dependent Refractive Index Sensitivities of Gold Nanocrystals with the Same Plasmon Resonance Wavelength. *J. Phys. Chem. C* **2009**, *113*, 17691−17697.

(8) Khalavka, Y.; Becker, J.; Sönnichsen, C. Synthesis of Rod-Shaped Gold Nanorattles with Improved Plasmon Sensitivity and Catalytic Activity. *J. Am. Chem. Soc.* **2009**, *131*, 1871−1875.

(9) Jain, P. K.; El-Sayed, M. A. Surface Plasmon Resonance Sensitivity of Metal Nanostructures: Physical Basis and Universal Scaling in Metal Nanoshells. *J. Phys. Chem. C* **2007**, *111*, 17451−17454.

(10) Xie, J.; Zhang, Q.; Lee, J. Y.; Wang, D. I. C. The Synthesis of SERS-Active Gold Nanoflower Tags for In Vivo Applications. *ACS Nano* **2008**, *2*, 2473−2480.

(11) Zhu, J.; Deng, X. C. Improve the Refractive Index Sensitivity of Gold Nanotube by Reducing the Restoring Force of Localized Surface Plasmon Resonance. *Sens. Actuators, B* **2011**, *155*, 843−847.

(12) Yu, C.; Irudayaraj, J. Multiplex Biosensor Using Gold Nanorods. *Anal. Chem.* **2006**, *79*, 572−579.

(13) Zheng, Y.; Thai, T.; Reineck, P.; Qiu, L.; Guo, Y.; Bach, U. DNA-Directed Self-Assembly of Core-Satellite Plasmonic Nanostructures: A Highly Sensitive and Reproducible Near-IR SERS Sensor. *Adv. Funct. Mater.* **2013**, *23*, 1519−1526.

(14) Rosman, C.; Prasad, J.; Neiser, A.; Henkel, A.; Edgar, J.; Sönnichsen, C. Multiplexed Plasmon Sensor for Rapid Label-Free Analyte Detection. *Nano Lett.* **2013**, *13*, 3243−3247.

(15) Waldeisen, J. R.; Wang, T.; Ross, B. M.; Lee, L. P. Disassembly of a Core−Satellite Nanoassembled Substrate for Colorimetric Biomolecular Detection. *ACS Nano* **2011**, *5*, 5383−5389.

(16) Sönnichsen, C.; Reinhard, B. M.; Liphardt, J.; Alivisatos, A. P. A Molecular Ruler Based on Plasmon Coupling of Single Gold and Silver Nanoparticles. *Nat. Biotechnol.* **2005**, *23*, 741−745.

(17) Wustholz, K. L.; Henry, A. I.; McMahon, J. M.; Freeman, R. G.; Valley, N.; Piotti, M. E.; Natan, M. J.; Schatz, G. C.; Duyne, R. P. V. Structure−Activity Relationships in Gold Nanoparticle Dimers and Trimers for Surface-Enhanced Raman Spectroscopy. *J. Am. Chem. Soc.* **2010**, *132*, 10903−10910.

(18) Yoon, J. H.; Lim, J.; Yoon, S. Controlled Assembly and Plasmonic Properties of Asymmetric Core−Satellite Nanoassemblies. *ACS Nano* **2012**, *6*, 7199−7208.

(19) Wang, C.; Du, Y.; Wu, Q.; Xuan, S.; Zhou, J.; Song, J.; Shao, F.; Duan, H. Stimuli-Responsive Plasmonic Core-Satellite Assemblies: i-motif DNA Linker Enabled Intracellular pH Sensing. *Chem. Commun.* **2013**, *49*, 5739−5741.

(20) Gandra, N.; Singamaneni, S. "Clicked" Plasmonic Core-Satellites: Covalently Assembled Gold Nanoparticles. *Chem. Commun.* **2012**, *48*, 11540−11542.

(21) Ross, B. M.; Waldeisen, J. R.; Wang, T.; Lee, L. P. Strategies for Nanoplasmonic Core-Satellite Biomolecular Sensors: Theory-Based Design. *Appl. Phys. Lett.* **2009**, *95*, 193112.

(22) Xu, L.; Hao, C.; Yin, H.; Liu, L.; Ma, W.; Wang, L.; Kuang, H.; Xu, C. Plasmonic Core−Satellites Nanostructures with High Chirality and Bioproperty. *J. Phys. Chem. Lett.* **2013**, *4*, 2379−2384.

(23) Chou, L. Y. T.; Zagorovsky, K.; Chan, W. C. W. DNA Assembly of Nanoparticle Superstructures for Controlled Biological Delivery and Elimination. *Nat. Nanotechnol.* **2014**, *9*, 148−155.

(24) Sebba, D. S.; Lazarides, A. A. Robust Detection of Plasmon Coupling in Core-Satellite Nanoassemblies Linked by DNA. *J. Phys. Chem. C* **2008**, *112*, 18331−18339.

(25) Wang, Z.; Zhang, J.; Ekman, J. M.; Kenis, P. J. A.; Lu, Y. DNA-Mediated Control of Metal Nanoparticle Shape: One-Pot Synthesis and Cellular Uptake of Highly Stable and Functional Gold Nanoflowers. *Nano Lett.* **2010**, *10*, 1886−1891.

(26) Gandra, N.; Abbas, A.; Tian, L.; Singamaneni, S. Plasmonic Planet−Satellite Analogues: Hierarchical Self-Assembly of Gold Nanostructures. *Nano Lett.* **2012**, *12*, 2645−2651.

(27) Koch, A. H. R.; Lévêque, G.; Harms, S.; Jaskiewicz, K.; Bernhardt, M.; Henkel, A.; Sönnichsen, C.; Landfester, K.; Fytas, G.

DOI: 10.1021/jp510985n
J. Phys. Chem. C 2015, 119, 5577−5582

Surface Asymmetry of Coated Spherical Nanoparticles. *Nano Lett.* **2014**, *14*, 4138−4144.
(28) Becker, J.; Schubert, O.; Sönnichsen, C. Gold Nanoparticle Growth Monitored in situ Using a Novel Fast Optical Single-Particle Spectroscopy Method. *Nano Lett.* **2007**, *7*, 1664−1669.
(29) Hanauer, M.; Pierrat, S.; Zins, I.; Lotz, A.; Sönnichsen, C. Separation of Nanoparticles by Gel Electrophoresis According to Size and Shape. *Nano Lett.* **2007**, *7*, 2881−2885.
(30) Becker, J.; Trügler, A.; Jakab, A.; Hohenester, U.; Sönnichsen, C. The Optimal Aspect Ratio of Gold Nanorods for Plasmonic Bio-sensing. *Plasmonics* **2010**, *5*, 161−167.
(31) Jakab, A.; Rosman, C.; Khalavka, Y.; Becker, J.; Trügler, A.; Hohenester, U.; Sönnichsen, C. Highly Sensitive Plasmonic Silver Nanorods. *ACS Nano* **2011**, *5*, 6880−6885.
(32) Schladt, T. D.; Shukoor, M. I.; Schneider, K.; Tahir, M. N.; Natalio, F.; Ament, I.; Becker, J.; Jochum, F. D.; Weber, S.; Köhler, O.; et al. Au@MnO Nanoflowers: Hybrid Nanocomposites for Selective Dual Functionalization and Imaging. *Angew. Chem., Int. Ed.* **2010**, *49*, 3976−3980.

DOI: 10.1021/jp510985n
J. Phys. Chem. C 2015, 119, 5577−5582